SMC-TR-03-14

AEROSPACE REPORT NO.
TR-2002(3397)-4

Capacity Trends in Nickel Electrodes as Affected by Temperature and Electrolyte Concentration

30 September 2002

Prepared by

L. H. THALLER, A. H. ZIMMERMAN, and G. A. TO
Electronics and Photonics Laboratory
Laboratory Operations

Prepared for

SPACE AND MISSILE SYSTEMS CENTER
AIR FORCE SPACE COMMAND
2430 E. El Segundo Boulevard
Los Angeles Air Force Base, CA 90245

National Systems Group

THE AEROSPACE CORPORATION
El Segundo, California

This report was submitted by The Aerospace Corporation, El Segundo, CA 90245-4691, under Contract No. F04701-00-C-0009 with the Space and Missile Systems Center, 2430 E. El Segundo Blvd., Los Angeles Air Force Base, CA 90245. It was reviewed and approved for The Aerospace Corporation by J. M. Williams, Principal Director, Programs & Technology Development Directorate, National Systems Group. Thomas Newbauer was the project officer.

This report has been reviewed by the Public Affairs Office (PAS) and is releasable to the National Technical Information Service (NTIS). At NTIS, it will be available to the general public, including foreign nationals.

This technical report has been reviewed and is approved for publication. Publication of this report does not constitute Air Force approval of the report's findings or conclusions. It is published only for the exchange and stimulation of ideas.

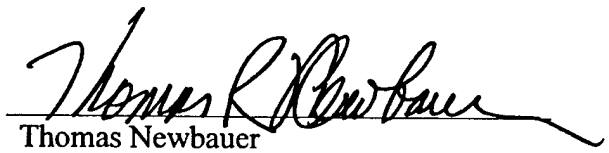

Thomas Newbauer
SMC/AXEN

REPORT DOCUMENTATION PAGE

Form Approved
OMB No. 0704-0188

1. REPORT DATE (*DD-MM-YYYY*)	2. REPORT TYPE	3. DATES COVERED (*From - To*)
30-09-2002		

4. TITLE AND SUBTITLE

Capacity Trends in Nickel Electrodes as Affected by Temperature and Electrolyte Concentration

5a. CONTRACT NUMBER
F04701-00-C-0009

5b. GRANT NUMBER

5c. PROGRAM ELEMENT NUMBER

6. AUTHOR(S)

L. H. Thaller, A. H. Zimmerman, and G. A. To

5d. PROJECT NUMBER

5e. TASK NUMBER

5f. WORK UNIT NUMBER

7. PERFORMING ORGANIZATION NAME(S) AND ADDRESS(ES)

The Aerospace Corporation
Laboratory Operations
El Segundo, CA 90245-4691

8. PERFORMING ORGANIZATION REPORT NUMBER

TR-2002(3397)-4

9. SPONSORING / MONITORING AGENCY NAME(S) AND ADDRESS(ES)

Space and Missile Systems Center
Air Force Space Command
2430 E. El Segundo Blvd.
Los Angeles Air Force Base, CA 90245

10. SPONSOR/MONITOR'S ACRONYM(S)
SMC

11. SPONSOR/MONITOR'S REPORT NUMBER(S)
SMC-TR-03-14

12. DISTRIBUTION/AVAILABILITY STATEMENT

Approved for public release; distribution unlimited.

13. SUPPLEMENTARY NOTES

14. ABSTRACT

An extensive review of the capacity trends of six representative nickel electrodes has been completed. The nickel electrodes were either taken from cells that had been successfully cycled for 40,000 simulated low Earth orbit cycles or were very new in terms of their life cycle history. One type of testing carried out on these electrodes determined their flooded capacity at four different temperatures under two different charging regimes when using two different electrolyte concentrations. The other type of testing determined the positions of the different charging peaks relative to the potential at which the co-evolution of oxygen becomes a significant factor during the charging process. The results of this study have explained why the use of certain temperatures and electrolyte concentrations can result in desirable or undesirable cell performance characteristics. The reasons behind two of the characteristic lower cell capacity phenomenon related to the use of 26% KOH vs. 31% KOH as the cell electrolyte concentration have become evident based on the results of this study.

15. SUBJECT TERMS

Nickel-hydrogen, Temperature effects, Capacity trends

16. SECURITY CLASSIFICATION OF:			17. LIMITATION OF ABSTRACT	18. NUMBER OF PAGES	19a. NAME OF RESPONSIBLE PERSON
a. REPORT	b. ABSTRACT	c. THIS PAGE			Lawrence Thaller
UNCLASSIFIED	UNCLASSIFIED	UNCLASSIFIED		28	19b. TELEPHONE NUMBER (*include area code*) (310)336-5180

Acknowledgement

The cycling data used in this report was made available from the life tests sponsored by the Air Force and NASA. The tests themselves were carried out at the Navy facility located at Crane, IN. Mr. Ralph James of the Air Force Research Laboratory in Albuquerque, NM was instrumental in authorizing access to the day-to-day cycling data that was collected and stored at the Navy testing facility. Mr. Thomas Miller of the NASA Glenn Research Center in Cleveland, OH was helpful in facilitating access to the NASA-funded cycling database information that was also collected and stored at the Navy facility.

Contents

Figures

Tables

1. Background

An ongoing study of the capacity trends and charging characteristics of a set of six representative nickel electrodes has been in progress for several years.[1,2,3] It was the goal to study four different cycling temperatures (24°, 10°, 0°, and –5°C) and two different electrolyte concentrations (26% and 31% KOH) with the help of two different electro-analytical techniques and relate these results to the performance of actual flight-weight IPV nickel-hydrogen cells. The electro-analytical techniques employed were the flooded utilization (FU) test and electrochemical voltage spectroscopy (EVS) test. In these earlier reports, based on the results of FU testing, it was shown that electrodes cycled in 31% KOH displayed more usable capacity than equivalent samples of electrode material cycled in 26% KOH solutions. EVS studies on samples of these representative electrodes showed that when nickel electrodes were cycled in 26% KOH solutions, they had a higher reversible potential than the same electrodes when cycled in 31% KOH solutions. As a consequence of this higher electrode potential, lower charging efficiencies were associated with cells using this lower electrolyte concentration since the co-evolution of oxygen occurs earlier in the recharge step compared with cells using 31% KOH as electrolyte.

It was also found that cycling electrodes at lower temperatures resulted in larger amounts of usable capacity since the kinetics of the oxygen evolution reaction were reduced, making the co-evolution of oxygen during the charging process less of a factor. At the time of the writing of the aforementioned references, not all of the electrodes had been tested at all the temperatures and in both electrolyte concentrations. Further use of these two electroanalytical techniques proved helpful in gathering the information that was needed to complete the latest phase of this study.

2. Introduction

FU and EVS testing have been carried out on a total of 48 samples of representative nickel electrodes. Analyses of these results have been incorporated into several prior reports.[1,2,3] Each of these reports has addressed a specific aspect or trend that has helped in the better understanding of actual nickel-hydrogen flight hardware. Now that the entire testing matrix has been completed, the data will be analyzed here with regard to the trends in usable capacity as affected by the cycling temperature and the concentration of electrolyte in which the electrodes were tested. Six representative electrodes were selected for this study. Nominal 1.0-cm^2 samples from the same parent electrode were used. Since no 3.5-in.- or 4.5-in.-dia electrode is completely homogenous, some degree of scatter is to be expected when comparing results from the six different electrodes tested under the same set of test conditions. For this reason, the general trends in the data will be viewed as more important than any one data point.

In viewing the trends in usable capacity as a function of temperature, an apparent anomaly was noted. The capacity trend associated with electrode samples cycled in 31% KOH solutions showed an increase as the temperature was reduced from 0°C to –5°C, whereas the capacity of samples tested in 26% KOH solutions displayed a sharp decrease. Since there is a continuing interest in the topic of 26% KOH vs. 31% KOH as the electrolyte of choice for nickel-hydrogen cells, a concerted effort was extended in this report to determine the reason for this apparent anomaly.

3. Description of Electrodes and Tests

3.1 The Electrodes

The electrodes used in these tests were standard, sintered nickel electrodes that had been removed from cells following life cycle testing or were new electrodes that had not yet been installed into cells. The electrodes used in these studies were selected based on coming from a wide variety of backgrounds in terms of cycling temperature, electrolyte concentration, number of accumulated charge/discharge cycles, and cobalt level in the active material. Table 1 summarizes the characteristics of the six sample electrodes. The ones that were removed from cells following cycling studies were still performing without any known performance problems. The sample sizes used in both the FU and the EVS studies were approximately 1.0 cm^2. Different samples from the same parent electrode were used for each FU or EVS test. Table 2 describes the matrix of tests that were carried out. All data have been normalized to 1.0 cm^2 sample sizes.

Table 1. Description of the Electrodes Used in the EVS and FU Studies

Plate No.	No. of Cycles	Approx. % Co	Cycling T, °C	Elect. Conc., % KOH	Rechg. Ratio, %
1	20	5	+20	31	Varied
2	40,000	5	+10	26	104
3	40,000	5	–5	26	103
4	40,000	10	+10	31	104
5	Not cycled	5	N.A.	N.A.	N.A.
6	Not cycled	10	N.A.	N.A.	N.A.

Table 2. Test Matrix for the FU and EVS Studies on the Set of Six Different Electrodes

Test Temperature	+24°C	+10°C	0°C	-5°C
Electrolyte Concentration	26% and 31% KOH	26% and 31% KOH	26% and 31% KOH	26% and 31% KOH

3.2 Flooded Utilization (FU) Tests

The FU test was used to avoid electrolyte concentration effects that might be experienced in an actual operating cell. In this test, a nominal 1.0-cm^2 sample of electrode was placed in a container containing about 100 ml of electrolyte of the concentration to be used for the test. The potential of the electrode was measured relative to a Hg/HgO reference electrode. The container was placed in a constant temperature chamber held at the test temperature by a thick copper cold plate. A coolant fluid was circulated through a serpentine copper coil that was soldered to the bottom of the cold plate.

During the test, the electrode undergoes three successive charge/discharge cycles. The tests are managed and the data collected and stored with the help of a computer. When considering a 30-mil thick electrode that is 82% porous and loaded with 1.65 g of active material per cc of void volume, the

theoretical capacity limits can be estimated. The weight of active material in one 50-cm^2 electrode would be 5.03 g. That would be equivalent to 1.45 Ah per plate if there would be a valence change of 1.0 (beta II to beta III reaction) and 2.43 Ah if there would be a valence change of 1.67 (beta II to gamma reaction). A 1.0-cm^2 sample of 30-mil electrode would contain between 29 and 49 mAh of theoretical capacity depending on whether it were fully charged to the beta phase or the gamma phase. Experience has shown that a fully charged sample of electrode material may contain as much as 36 mAh of usable capacity and 40 mAh of total capacity.

The first charge cycle (4 mA for 10 h) in the FU test sequence is used to convert the less active form[4] of the active material into the more active form that is seen during normal charging and discharging of the active material. Prior to the second charge cycle, the electrode was fully discharged in three steps. During the first step, the electrode was discharged at the rate of 10 mA to a 1.0-V cutoff. This corresponds to about the C/4 rate if the electrode were in an actual nickel-hydrogen cell. The capacity at this rate is defined in these tests as the "useable capacity." Following this first step of the discharge process, the electrode was discharged further at the 2-mA rate to a –0.5-V cutoff. This capacity is referred to as the "residual capacity." The next step in the discharge was conducted at the 0.2-mA rate to a –0.5-V cutoff. This capacity is referred to as the "unavailable capacity." The sum of these three capacity elements is referred to as the "total capacity."

During the second cycle, the electrode was first charged at approximately the C/10 rate for 10 h (4 mA). Following this charging step, the active material was still mostly in the beta phase of the charged active material. Following another three-step discharge sequence, a third charging step was carried out. In this step, the C/10 charging rate is carried out for 14 h. This will charge different amounts of the active material to the gamma phase. This form of the active material contains a larger amount of capacity since the average valance of the nickel ions in the gamma form is 3.66 as opposed to 3.0 for the beta-phase form of the active material. The amount of active material that is converted to the gamma phase will depend on the charging potential of that material relative to the oxygen evolution characteristics of that electrode. A typical trace of the electrode potential vs. an Hg/HgO reference electrode for a FU test is shown in Figure 1.

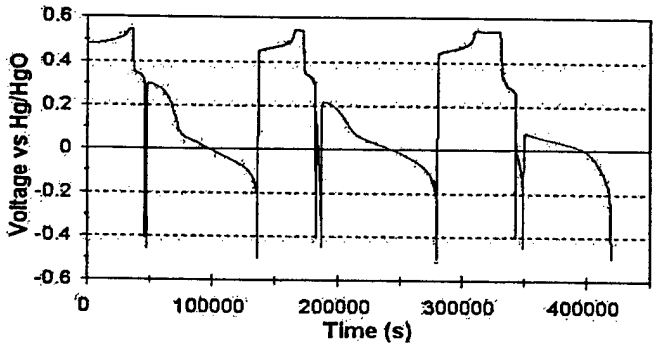

Figure 1. Typical voltage trace of a Flooded Utilization test.

3.3 Electrochemical Voltage Spectroscopy (EVS) Test

EVS testing was carried out in parallel with the samples tested using the FU technique. The setup for this test was very similar to that used for the FU test. A nominal 1.0-cm^2 sample of electrode was immersed in a container containing about 100 ml of electrolyte of the concentration to be used in the test. Its potential was measured relative to a Hg/HgO reference electrode. The container was placed in a constant-temperature chamber held at the test temperature by a thick copper cold plate. A coolant fluid was circulated through a serpentine copper coil that was soldered to the bottom of the cold plate. Unlike the charging and discharging step in the FU test, the voltage in the EVS test was increased or decreased much more slowly. In the tests to be described here, the voltage was changed at the rate of 2 μV/s. The test results are very similar to what would be obtained using the sweep voltammeter technique.

After a sample was placed in the test cell, the voltage was first decreased to 0.2 V at the rate of 2 μV/s to completely discharge all of the active material. Next, the voltage was increased at the rate of 2 μV/s to the end-of-charge voltage. The amount of charge that was consumed during the charging process is the integrated area under the curve. During the first charging scan, the active material was still in the less active form since the electrode had been at rest for a number of weeks. As the charging voltage approaches the end-of-charge potential, the electrode enters a region where oxygen evolution and charging of some of the active material occur in parallel. In these tests, the end-of-charge voltage was set high enough to be assured that the electrode reached the potential where oxygen evolution was the major reaction. Upon reaching the end-of-charge voltage, the voltage was reduced at the rate of 2 μV/s. Upon reaching about 0.35 V, the higher voltage beta material was first discharged, followed by the gamma-phase material at about 0.29 V. After again reaching 0.2 V, a second cycle was carried out.

Figure 2 shows the results of a typical EVS test. In this particular test, all of the active material was charged to the gamma phase. The difference between the first and second charging portions of the scans (the area below zero) is quite noticeable. During the first scan, a higher voltage is required to convert the active material that has been at rest for weeks or months into the modified crystal structure that is charged at a lower voltage during the second scan.[4] Earlier EVS studies with these same

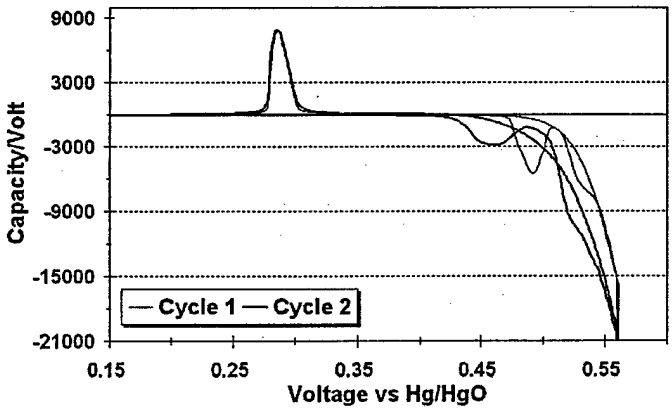

Figure 2. Typical results from an EVS test using a first and second scan.

electrodes[1,2,3] found that the position of the charging peaks relative to the oxygen evolution characteristics of each of these tests was slightly different. They depended on the cycling temperature, number of accumulated charge/discharge cycles, the electrolyte concentration, and the level of cobalt additive in the active material.[1]

4. Capacity Trends with Temperature and Electrolyte Concentration

During the course of a single FU test, six different mAh capacities are recorded automatically as part of the computer-controlled FU equipment. Three capacities were measured following the second 10-h charge cycle (after the 10 mA, 2 mA, and 0.2 mA discharge periods) and three following the 14-h charge cycle (after the 10 mA, 2 mA, and 0.2 mA discharge periods). In the following tables and charts, the usable capacities (at 10 mA/cm^2) and the sum of the three portions of the total capacity following the two different charge steps will be used in the figures that will be presented. For each of the six different electrodes there will be values when tested in the two different electrolyte concentrations and at the four different test temperatures. The Appendices contain a complete set of the FU data collected during these tests.

The results shown in Figures 3 and 4, which are typical of the results of the other five electrodes, indicate an increase in usable as well as total capacity in electrodes cycled in 31% KOH as the temperature is lowered from 0° to –5°C, whereas there is a reduction in capacity from 0° to –5°C when 26% KOH is used as the electrolyte. The spans in capacity between that obtained at the 10 mA rate (the usable capacity) and the total of the three portions of the total capacities obtained at the three discharge rates are about the same in all cases. The divergence in capacities as –5°C was a significant finding since it was found earlier that as the temperature was lowered, the kinetics of the oxygen evolution reaction was reduced.[1]

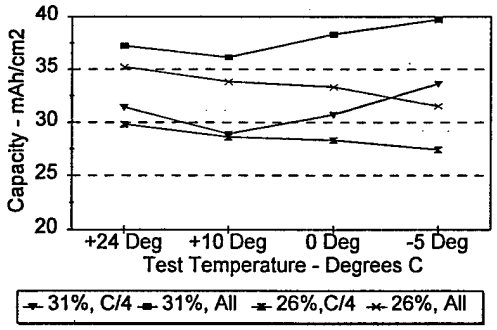

Figure 3. Set of FU results for Plate No. 1 electrodes following the 10-h charge cycle.

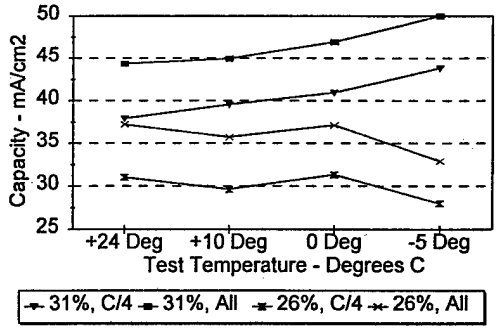

Figure 4. Set of FU results for Plate No. 1 electrodes following the 14-h charge cycle.

5. Explanations for the Low Temperature Capacity Trends In 26% KOH Electrolytes

An explanation of this unexpected turnabout in capacity/temperature relationship begins with an illustrative figure showing the potentials and relative positions of the different charging and discharging reactions. Figure 5 may be understood as follows. It is well established that during the charging of nickel electrodes from a fully discharged condition, the active material is first charged to the beta phase as the average valence of the nickel changes from +2 to +3 (the peak at about 0.45 V). Following this, some of the material can be charged to the gamma phase where the average valence of the nickel is +3.66 (the peak at about 0.53V). This second process often occurs in parallel with the evolution of oxygen at the nickel electrode (the line extending down to about 0.54 V). To increase the usable energy density of the nickel electrode and at the same time to minimize the damage to the electrode and increase the charge efficiency of the charging step, there should be as wide a separation as possible between the potential at which the active material is charged to the gamma phase and the potential at which large amounts of oxygen are evolved. However, at the cycling temperatures in common use, these latter two reactions generally occur in parallel at about the same potential.

During the discharge portion of the cycle, the material that is in the beta phase will discharge first since the voltage at which it discharges is higher than the voltage at which the gamma-phase material discharges. The peaks for these processes occur at about 0.35 V for the discharge of the beta material and 0.28 V for the discharge of the gamma-phase material. The relative amounts of beta and gamma material depend on the recharge ratio, end-of-charge voltage, the exact positions of the beta and gamma charging peaks, the cobalt additive level in the active material, and cycling temperature employed during the charging step. When electrode material is cycled at temperatures and charging rates usually seen in actual cell cycling, the gamma charging peak moves to the right and is often seen only as a shoulder on the oxygen evolution curve.

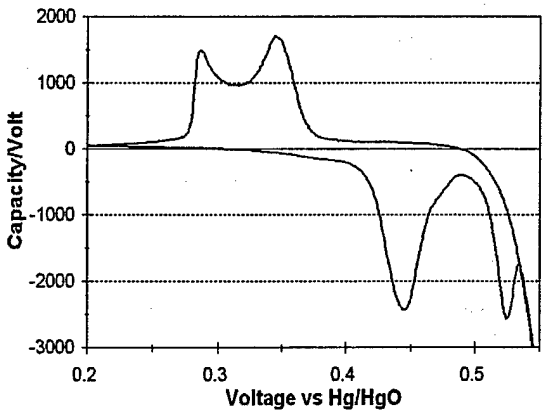

Figure 5. Major charging and discharge features available from an EVS scan.

Figures 6 and 7 provide valuable information to help explain the down turn in capacity at –5°C when using 26% KOH as the electrolyte as well as the lower amounts of usable capacity at all temperatures compared with the equivalent electrodes tested in 31% KOH solutions. Viewed side by side, it can be seen that all of the dischargeable material in the electrode cycled in 31% KOH had been charged to the gamma phase, whereas the majority of the dischargeable material in the electrode cycled in 26% KOH is still in the beta phase. The integrated area under the curve for the gamma-phase discharge (48.5 mAh) is noticeably larger than the area under the discharge curve of the mixed-phase discharge (32.6 mAh). During the charging portion of the electrode in 31% KOH, a clear peak related to charging to the gamma phase is seen, while this peak is absent from the charging portion of the electrode cycled in 26% KOH. Also to be noted is the higher potential of the charging peak of the reaction related to the charging to the beta phase that is associated with the electrode cycled in 26% KOH.

The first step in quantifying these general observations of Figures 6 and 7 is to locate the positions of the beta charging peaks during the second scan for each of the 48 different EVS tests. These values are recorded in Tables 3 and 4.

5.1 Beta Peak Positions

In this section, the data from all of the EVS scans were reviewed and the different positions of the charging peaks were located. What will be called the oxygen evolution characteristic will be the potential where the oxygen evolution rate was equal to 1000 mAh/V during the beginning of the scan after reaching the end-of-charge voltage of the second scan. From this information, the Tables 3 and 4 were developed.

The major observation in these tables when comparing the tests carried out with 26% KOH and the equivalent test with 31% KOH is the higher voltages associated with the beta charging peaks of the tests that used 26% KOH. The values associated with Plate No. 6 are noticeable lower than for the other five plates. This difference stemmed from the fact that this electrode was manufactured with a cobalt additive level of about 10%, whereas Plates Nos. 1, 2, 3, and 5 were manufactured with cobalt additive levels of closer to 5%. Plate No. 4 was also manufactured with about 10% cobalt, but after about 40,000 LEO cycles, the 20 to 25% plaque corrosion that took place disrupted the original cobalt concentrations. Plate No. 5 now acts very similar to electrodes that were manufactured with 5% cobalt levels.

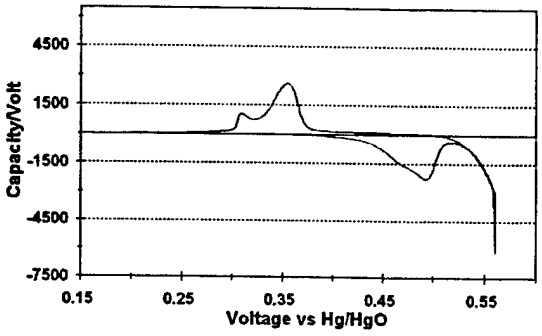

Figure 6. EVS scan at -5°C in 26% KOH

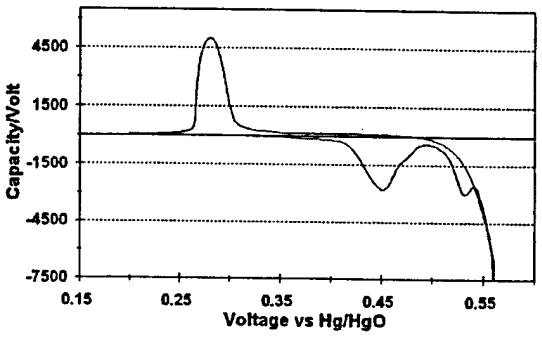

Figure 7. EVS scan at -5°C in 31% KOH

Table 3. The Positions of the Beta Charging Peaks (vs. Hg/HgO Reference) During the Second EVS Scan as a Function of Temperature for Tests Using 31% KOH as the Electrolyte

Plate No.	31%, –5°C	31%, 0°C	31%, +10°C	31%, +24°C
1	0.451	0.452	0.449	0.452
2	0.450	0.451	0.452	0.457
3	0.442	0.441	0.438	0.450
4	0.445	0.446	0.448	0.456
5	0.442	0.450	0.449	0.450
6	0.412	0.412	0.409	0.408

Table 4. The Positions of the Beta Charging Peaks (vs. a Hg/HgO Reference) During the Second EVS Scan as a Function of Temperature for Tests Using 26% KOH as the Electrolyte

Plate No.	26%, –5°C	26%, 0°C	26%, +10°C	26%, +24°C
1	0.492	0.495	0.469	0.459
2	0.475	0.492	0.468	0.468
3	0.476	0.485	0.456	0.464
4	0.496	0.497	0.462	0.463
5	0.483	0.465	0.457	0.459
6	0.429	0.430	0.430	0.413

5.2 Potential Spans Between the Beta Peak and the Oxygen Evolution Characteristic

Tables 5 and 6 tabulate the differences between the voltage where the oxygen evolution rate equaled 1000 during the second EVS scan and the voltage describing the position of the peak of the beta charging reaction. This difference is viewed to be the span between charging to the beta phase and where the evolution of oxygen becomes significant. The larger the span between these two potentials, the larger is the amount of active material that will be charged prior to the onset of an excessive rate of oxygen evolution.

Table 5. The Difference Between the Oxygen Evolution Characteristic and the Location of the Beta Charging Peak During the Second EVS Scan for the Tests Using 31% KOH

Plate No.	31%, –5°C	31%, 0°C	31%, +10°C	31%, +24°C
1	0.079	0.086	0.069	0.030
2	0.084	0.095	0.067	0.017
3	0.093	0.106	0.073	0.030
4	0.086	0.100	0.072	0.022
5	0.078	0.083	0.058	0.003
6	0.126	0.100	0.111	0.067

Table 6. The Difference Between the Oxygen Evolution Characteristic and the Location of the Beta Charging Peak During the Second EVS Scan for the Tests Using 26% KOH

Plate No.	26%, –5°C	26%, 0°C	26%, +10°C	26%, +24°C
1	0.050	0.045	0.043	0.008
2	0.030	0.043	0.040	-0.006
3	0.031	0.062	0.044	0.004
4	0.054	0.045	0.036	0.009
5	0.048	0.062	0.048	0.003
6	0.111	0.108	0.088	0.062

Tables 5 and 6 show, as expected, a greater span as one lowers the temperature below room temperature. This would suggest a larger amount of electrochemical capacity as the temperature is lowered. By comparing Table 5 with Table 6, there is a larger span associated with electrodes that are tested in 31% KOH solutions. The values for the span associated with Plate No. 6 are consistently higher than those of the other five plates. This is attributed to the electrode having a cobalt additive concentration of about 10%. A higher cobalt level results in a lower electrode potential relative to electrodes that are manufactured with 5% cobalt. This will result in higher charging efficiencies when using electrodes with higher cobalt contents.

5.3 Gamma Peak Positions

Table 7 lists the positions of the gamma charging peaks for the 24 tests using the EVS technique with tests that employed 31% KOH as the electrolyte concentration. To be noted is the movement in the position of the gamma peak first towards higher voltages and then towards lower voltages at the –5°C test set. No such table could be developed for the 26% KOH set of tests since there were no distinct gamma peaks at any of the four test temperatures. At room temperature, there were some minor shoulders as the electrode was transitioning to oxygen evolution. An estimate of the position of the gamma peak at +24°C for the 26% KOH test was 0.525 V. This was about 15 mV closer to the position of the oxygen evolution characteristic than tests in 31% KOH and would suggest a reduction in the amount of gamma-phase formation in the lower electrolyte concentration tests.

Table 7. The Positions of the Gamma Charging Peaks (vs. Hg/HgO Reference) During the Second EVS Scan as a Function of Temperature When Using 31% KOH as the Electrolyte

Plate No.	31%, –5°C	31%, 0°C	31%, +10°C	31%, +24°C
1	0.532 V	0.542 V	0.517 V	None
2	0.527 V	0.538 V	0.516 V	0.510 V
3	0.530 V	0.538 V	0.514 V	None
4	0.525 V	0.536 V	0.513 V	0.510 V
5	0.528 V	0.539V	0.517 V	None
6	None	None	None	None

5.4 Capacity Increases due to Overcharge

Table 8 was generated from the results of the FU testing program. The results presented in the table review the amounts of usable capacity obtained from the set of six plate samples cycled in 31% KOH. These capacity values were obtained following 10 h of charge at about the C/10 rate and following 14 h of charge also at the C/10 rate—all at –5°C. The last column calculates the percent increase in usable capacity following four extra hours of charging. Since a 1.0-cm^2 piece of electrode contains about 30 mAh when charged to the beta phase and about 50 mAh when charged to the gamma phase, it is evident from this table that under these conditions various amounts of gamma-phase material are formed during the 14-h charge period.

Table 9 contains the equivalent results for electrode samples tested in 26% KOH. It is evident that except for Plate No. 2 there was very little gain in usable capacity following the extensive amount of overcharge employed in the test. The capacity values in Table 9 indicate that very little, if any, of the active material was charged to the gamma phase during the overcharge applied during the 14-h charge cycle.

Table 8 shows higher capacities than seen in Table 9, and,in addition, significant amounts of capacity increase during the 14-h charge period. The presence of a clear gamma-phase charging peak in the EVS scan of the electrode tested in 31% KOH (Figure 7) was responsible for the presence of these higher capacity values during the FU testing.

Table 8. Capacities During the 10 mA Discharges of the Six Different Representative Electrodes at –5°C and in 31% KOH

Plate No.	Cap at 10 mA rate After 10-h charge - mAh	Cap at 10 mA rate After 14-h charge - mAh	Percent Capacity Increase
1	33.6	43.8	30.4%
2	32.8	40.9	24.7%
3	31.0	39.6	27.7%
4	28.9	40.5	40.1%
5	32.9	39.8	21.0%
6	33.8	41.1	21.6%

Table 9. Capacities During the 10-mA Discharges of the Six Different Representative Electrodes at –5°C and in 26% KOH

Plate No.	Cap at 10 mA rate After 10-h charge - mAh	Cap at 10 mA rate After 14-h charge - mAh	Percent Capacity Increase
1	27.4	28.0	2.2%
2	18.8	23.0	22.3%
3	22.2	22.9	3.2%
4	24.1	25.1	4.1%
5	23.9	25.1	5.0%
6	23.7	26.5	11.8%

5.5 Capacity Gains Using 31% KOH vs. 26% KOH

In Table 10, the larger amounts of capacity that are available when using 31% KOH vs. 26% KOH as the electrolyte in tests carried out at –5°C are clearly evident. Reference 2 explained that at test temperatures around +10°C there is more walkdown associated with 26% KOH solutions vs. 31% KOH solutions because in 26% KOH solutions the reversible potential of a nickel electrode is closer to where oxygen is evolved and thus the charging efficiency is lower. At –5°C it appears that it is ultra difficult to charge the beta material to the gamma phase since the position of the gamma peak is imbedded in the process where oxygen evolution is occurring much more rapidly than the beta material can be converted to the gamma phase. It is difficult to differentiate whether the reversible potential of the gamma reaction moves to higher voltages as the temperature is lowered or whether the kinetics of the gamma charging reaction are depressed.

Table 10. FU Capacity Gains in Nickel Electrodes When Using 31% vs. 26% KOH Electrolytes Solutions Following 10 h and 14 h of Charging When Tested at –5°C

Plate No.	After 10 h of charge	After 14 h of charge
1	22.6%	56.4%
2	74.5%	77.8%
3	39.6%	72.9%
4	19.9%	61.4%
5	37.6%	58.6%
6	42.6%	55.1%

6. Relevance of Results to Actual Cell Performance

One of the better performing cell packs involved in the Air Force-supported cycling studies carried out at the Navy facility located in Crane, IN showed no capacity walkdown during over 40,000 LEO cycles.[1] The cell had been cycled at –5°C with a recharge ratio (RR) of about 1.03. The cell contained 40, 3.5-in.-dia plates that were about 30 mils in thickness. The cell was activated with 26% KOH as the electrolyte. A similar cell pack filled with 26% KOH, but cycled at +10°C, showed a considerable amount of capacity walkdown as estimated by the drop in pressure at the end of the charging step.[1] By converting this loss of end-of-charge pressure to Ah of capacity, the cell cycled at +10°C lost about 30 to 40% of the capacity it had at the beginning of the test. Figures 8 and 9 show a pair of typical charge and discharge cycles obtained from each of these two cell packs following the stabilization in the end-of-charge pressure of the cell that was cycled at +10°C.

The much sharper turn-up of the charging curve for the cell cycled at –5°C is clearly seen by comparing these two figures. This is indicative of a smaller amount of transition into oxygen evolution and thus a higher charge efficiency, resulting in a higher state-of-charge at the end of the charging period even though a smaller amount of recharge was charged back into the cell cycling at –5°C. The upward displacement of both the EOD voltage and the EOC of the cell cycling at –5°C is due in part to the change in reversible potential of nickel-hydrogen cells with temperature (about 1.0 mV/°C) and in part due to the higher states-of-charge at both the end-of-discharge and the end-of-charge. The reduced kinetics of the oxygen evolution reaction at this lower temperature permits a greater percentage of the charging current to be used for the charging of the active material. Two cells from each of these ten-cell packs were made available for further study in our laboratory.[4] The results of that portion of this study were reviewed in an earlier report.

Following over 40,000 LEO cycles, post-test capacity checks were carried out at the Navy facility in Crane, IN on both of these cells. Following a complete letdown and a single recharge of 63.8 Ah, 50.2 Ah of usable capacity (C-rate) and 9.0 Ah of residual capacity (C/10) were obtained from the cell that had been cycled at –5°C. Plate material from one of these cells in this 10-cell pack was

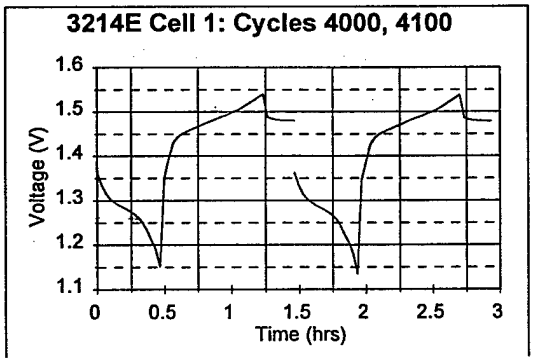

Figure 8. Cycling at +10°C and 1.04 RR.

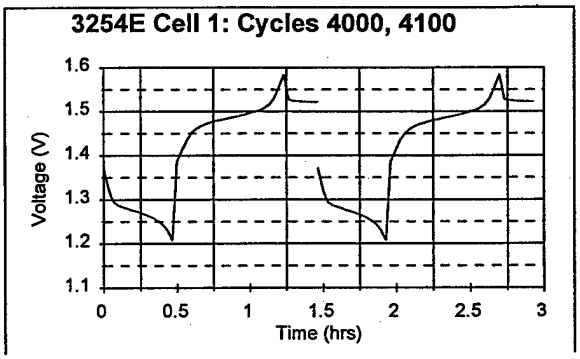

Figure 9. Cycling at –5°C and 1.03 RR.

made available to us for further testing and is identified in these studies as Plate No. 3. The FU test results recorded a usable capacity (C/4 to 1.0V) of only 22.2 mAh/cm^2 of electrode surface. The data from the FU and EVS testing would suggest that at this cycling temperature and this electrolyte concentration a very low level of usable capacity compared with other possible conditions would result. In a 40-plate cell with 3.5-in.-dia electrodes, there are approximately 2000 cm^2 of active plate area. Projecting the 22.2 mAh/cm^2 value to a full cell would suggest 44.4 Ah for the full cell when given minimal amounts of overcharge. The actual cell delivered 50.2 Ah. If the actual internal components of a cell operating in a –5°C chamber are closer to 0°C, the projected cell usable capacity based on this FU study would be 50.4 Ah, which would be equal to the 50-Ah nameplate capacity of this cell and close to the value obtained in the Crane, post-test determination.

Figures 10 and 11, featuring the results for Plate No. 3, are similar to Figures 3 and 4, where the capacity trends are plotted as a function of the different test parameters. Plate No. 3 is typical of an electrode that had successfully completed 40,000 simulated LEO cycles. It shows the same increasing capacity trend as the temperature is decreased to –5°C when using 31% KOH as the electrolyte, while there is a sharp decrease in capacity at –5°C when 26% KOH was used as the electrolyte.

A further difference that was noted between the results of the FU testing and actual cell performance was related to the very high states-of-charge that could be attained in the FU tests at low temperatures. Referring back to Figures 3 and 4, a FU capacity of from 40 to 50 mAh/cm^2 would correspond to 80 to 100 Ah of capacity in a 2000-cm^2 cell. It is unusual to exceed 60 to 65 Ah in a fully charged cell having a nameplate capacity of 50 Ah. The FU technique must permit a very efficient utilization of most of the active material. Plate No. 1, which formed the basis for Figures 3 and 4, was a 35-mil electrode. This thickness suggests that if the active material had been completely converted to the gamma phase, the unit capacity would be 57 mAh/cm^2. Based on these numbers, the nameplate rating on cells corresponds to the active material being charged to below the level where all of the active material would all be in the charged beta state.

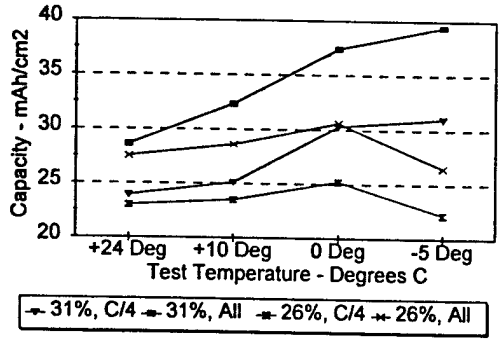

Figure 10. Set of FU results for Plate No.3 electrodes following the 10-h charge cycle.

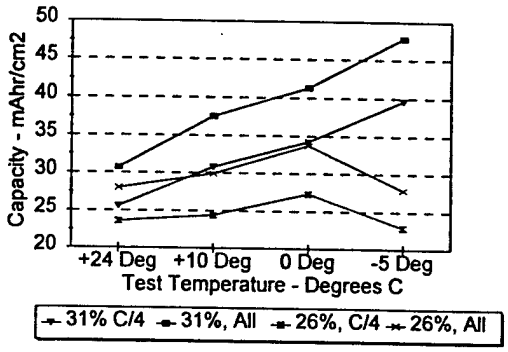

Figure 11. Set of FU results for Plate No.3 electrodes following the 14-h charge cycle

7. Summary

The summary results from an extensive test program have been reviewed as they relate to the capacity trends of sample nickel electrodes. One-cm^2 samples of six representative nickel electrodes were tested at four different temperatures and in two different electrolyte concentrations. It was noted that at –5°C, electrode samples tested in 26% KOH experienced a drop in usable capacity compared to electrode samples tested in 31% KOH, which showed an increase in usable capacity. A close examination of this phenomenon showed that under these conditions of temperature and electrolyte concentration, it is very difficult to charge the beta-phase material to the gamma phase due to the interference of the co-evolution of oxygen. The longevity characteristics of nickel electrodes when cycled for tens of thousand of cycles in 26% KOH electrolyte solutions must stem from the inability to form significant amounts of gamma-phase material. It has been demonstrated in previous studies that the formation of large amounts of gamma-phase material results in plate expansion due to the larger lattice constants of the gamma-phase structure compared to the beta-phase material.

References

1. Thaller, L. H., Zimmerman, A. H., and To, G. A., "Techniques to Improve the Usability of Nickel-Hydrogen Cells," Aerospace Report No. TR-2002(3397)-2, 1 May 2002.

2. Thaller, L. H., Zimmerman, A. H., and To, G. A., "Understanding and Managing Capacity Walkdown in Nickel-Hydrogen Cells and Batteries," Aerospace Report No. TR-2002(3000)-2, 31 May 2002.

3. Thaller, L. H., Zimmerman, A. H., and To, G. A., "Flooded Utilization and Electrochemical Voltage Spectroscopy Studies on Nickel Electrodes," Aerospace Report No. TR-2002(3397)-3, 1 July 2002.

4. Thaller, L. H., Zimmerman, A. H., and To, G. A., "Capacity Management and Walkdown During LEO Cycling of Nickel-Hydrogen Cells and Batteries," Aerospace Report No. TR-2001(3010)-1, October 2000.

Appendix 1. Summary of FU Results of Tests Conducted in 31% KOH

Electrode	Current, mA	31% @ 24°C	31% @10°C	31% @ 0°C	31% @ –5°C
Plate No. 1	10.0	31.4	28.9	30.7	33.6
10-h chg.	2.0	3.2	3.2	2.4	0.9
	0.2	2.6	3.9	5.1	5.2
	Total	37.2	36.0	38.3	39.7
	10.0	37.9	39.5	40.9	43.8
14-h chg.	2.0	3.9	2.8	3.3	0.7
	0.2	2.5	2.6	2.6	5.5
	Total	44.3	44.9	46.9	50.0
Plate No. 2	10.0	26.9	27.5	30.3	32.8
10-h chg.	2.0	3.1	2.0	1.2	2.5
	0.2	1.8	4.0	5.3	6.2
	Total	31.8	33.5	36.8	41.5
14-h chg.	10.0	30.5	32.9	35.7	40.9
	2.0	3.2	2.9	2.0	3.4
	0.2	2.0	3.1	3.7	4.9
	Total	35.7	38.9	41.4	49.2
Plate No. 3	10.0	23.9	25.1	30.3	31.0
10-h chg.	2.0	2.5	2.6	2.8	2.7
	0.2	2.2	4.6	4.2	5.7
	Total	28.6	32.3	37.4	39.4
	10.0	25.6	30.8	34.2	39.6
14-h chg.	2.0	2.8	2.9	3.3	3.9
	0.2	2.3	3.8	3.8	4.3
	Total	30.7	37.5	41.3	47.8
Plate No. 4	10.0	26.9	29.4	36.6	28.9
10-h chg.	2.0	3.1	1.7	0.3	0.8
	0.2	2.8	4.3	2.5	4.0
	Total	32.8	35.4	39.4	33.7
	10.0	30.5	36.6	38.4	40.5
14-h chg.	2.0	3.2	1.6	0.2	0.3
	0.2	4.0	3.9	2.5	3.0
	Total	37.7	42.1	41.2	43.8
Plate No. 5	10.0	26.9	30.2	33.0	32.8
10-h chg.	2.0	3.1	1.6	2.8	2.0
	0.2	1.8	3.3	3.4	4.5
	Total	31.8	35.1	39.2	39.3
	10.0	30.5	35.8	32.9	39.8
14-h chg.	2.0	3.2	2.0	1.1	1.6
	0.2	2.0	2.7	0.5	5.1
	Total	35.7	40.5	34.5	46.5

Electrode	Current, mA	31% @ 24°C	31% @10°C	31% @ 0°C	31% @ –5°C
Plate No. 6	10.0	27.7	29.0	36.7	33.8
10-h chg.	2.0	2.9	1.6	3.1	1.4
	0.2	1.8	3.0	2.8	4.5
	Total	32.4	33.6	42.6	39.7
	10.0	32.1	33.7	34.3	41.1
14-h chg.	2.0	3.1	2.1	1.3	1.8
	0.2	1.6	2.6	4.3	4.1
	Total	36.8	38.4	39.9	47.0

Appendix 2. Summary of FU Results of Tests Conducted in 26% KOH

Electrode	Current, mA	26% @24°C	26% @10°C	26% @ 0°C	26% @ –5°C
Plate No. 1	10.0	29.8	28.6	28.3	27.4
10-h chg.	2.0	3.2	1.0	0.7	0.5
	0.2	2.2	4.2	4.3	3.6
	Total	35.2	33.8	33.3	31.5
	10.0	31.0	29.6	31.3	28.0
14-h chg.	2.0	3.5	1.3	0.9	0.7
	0.2	2.7	4.8	4.8	4.2
	Total	37.2	35.7	37.1	32.9
Plate No. 2	10.0	25.3	22.8	24.6	18.8
10-h chg.	2.0	2.8	1.8	1.1	1.2
	0.2	2.6	4.1	4.5	4.0
	Total	30.7	28.7	30.1	24.0
14-h chg.	10.0	27.1	26.1	29.1	23.0
	2.0	2.6	2.0	1.0	1.1
	0.2	3.1	3.9	4.6	4.3
	Total	32.8	32.0	34.8	28.4
Plate No. 3	10.0	23.0	23.5	25.2	22.2
10-h chg.	2.0	2.2	1.7	1.1	0.6
	0.2	2.3	3.4	4.2	3.7
	Total	27.5	28.6	30.6	26.5
	10.0	23.6	24.4	27.3	22.9
14-h chg.	2.0	2.1	2.0	1.6	0.9
	0.2	2.3	3.5	4.8	4.1
	Total	28.0	29.9	33.7	27.9
Plate No. 4	10.0	27.0	24.0	25.1	24.1
10-h chg.	2.0	1.8	0.4	0.3	3.4
	0.2	4.0	2.3	2.2	1.6
	Total	32.8	26.7	27.6	29.1
	10.0	29.7	23.5	27.0	25.1
14-h chg.	2.0	1.8	0.7	0.6	0.3
	0.2	4.3	4.5	3.7	1.8
	Total	35.7	28.7	31.4	27.2
Plate No. 5	10.0	27.1	26.2	25.0	23.9
10-h chg.	2.0	3.3	1.4	0.8	0.9
	0.2	2.3	2.9	3.4	3.2
	Total	32.8	30.5	29.3	28.0
	10.0	28.6	28.2	27.4	25.1
14-h chg.	2.0	3.7	1.5	0.0	1.0
	0.2	2.1	3.1	4.5	3.4
	Total	34.4	32.8	31.9	29.5

Electrode	Current, mA	26% @24°C	26% @10°C	26% @ 0°C	26% @ –5°C
Plate No. 6	10.0	25.2	26.0	24.5	23.7
10-h chg.	2.0	2.8	1.6	1.1	1.2
	0.2	2.1	3.2	3.9	4.3
	Total	30.1	30.8	29.5	29.2
	10.0	26.8	28.5	27.6	26.5
14-h chg.	2.0	2.9	1.6	1.1	1.0
	0.2	2.1	3.1	3.8	4.2
	Total	31.8	33.2	32.5	31.7

Appendix 3. Side by Side FU Results at –5°C

Electrode	31% @ –5°C	26% @ –5°C
Plate No. 1	33.6	27.4
10-h chg.	0.9	0.5
	5.2	3.6
	39.7	31.5
	43.8	28.0
14-h chg.	0.7	0.7
	5.5	4.2
	50.0	32.9
Plate No. 2	32.8	18.8
10-h chg.	2.5	1.2
	6.2	4.0
	41.5	24.0
14-h chg.	40.9	23.0
	3.4	1.1
	4.9	4.3
	49.2	28.4
Plate No. 3	31.0	22.2
10-h chg.	2.7	0.6
	5.7	3.7
	39.4	26.5
	39.6	22.9
14-h chg.	3.9	0.9
	4.3	4.1
	47.8	27.9
Plate No. 4	28.9	24.1
10-h chg.	0.8	3.4
	4.0	1.6
	33.7	29.1
	40.5	25.1
14-h chg.	0.3	0.3
	3.0	1.8
	43.8	27.2
Plate No. 5	32.8	23.9
10-h chg.	2.0	0.9
	4.5	3.2
	39.3	28.0
	39.8	25.1
14-h chg.	1.6	1.0
	5.1	3.4
	46.5	29.5

Electrode	31% @ –5°C	26% @ –5°C
Plate No. 6	33.8	23.7
10-h chg.	1.4	1.2
	4.5	4.3
	39.7	29.2
	41.1	26.5
14-h chg.	1.8	1.0
	4.1	4.2
	47.0	31.7

LABORATORY OPERATIONS

The Aerospace Corporation functions as an "architect-engineer" for national security programs, specializing in advanced military space systems. The Corporation's Laboratory Operations supports the effective and timely development and operation of national security systems through scientific research and the application of advanced technology. Vital to the success of the Corporation is the technical staff's wide-ranging expertise and its ability to stay abreast of new technological developments and program support issues associated with rapidly evolving space systems. Contributing capabilities are provided by these individual organizations:

Electronics and Photonics Laboratory: Microelectronics, VLSI reliability, failure analysis, solid-state device physics, compound semiconductors, radiation effects, infrared and CCD detector devices, data storage and display technologies; lasers and electro-optics, solid state laser design, micro-optics, optical communications, and fiber optic sensors; atomic frequency standards, applied laser spectroscopy, laser chemistry, atmospheric propagation and beam control, LIDAR/LADAR remote sensing; solar cell and array testing and evaluation, battery electrochemistry, battery testing and evaluation.

Space Materials Laboratory: Evaluation and characterizations of new materials and processing techniques: metals, alloys, ceramics, polymers, thin films, and composites; development of advanced deposition processes; nondestructive evaluation, component failure analysis and reliability; structural mechanics, fracture mechanics, and stress corrosion; analysis and evaluation of materials at cryogenic and elevated temperatures; launch vehicle fluid mechanics, heat transfer and flight dynamics; aerothermodynamics; chemical and electric propulsion; environmental chemistry; combustion processes; space environment effects on materials, hardening and vulnerability assessment; contamination, thermal and structural control; lubrication and surface phenomena.

Space Science Applications Laboratory: Magnetospheric, auroral and cosmic ray physics, wave-particle interactions, magnetospheric plasma waves; atmospheric and ionospheric physics, density and composition of the upper atmosphere, remote sensing using atmospheric radiation; solar physics, infrared astronomy, infrared signature analysis; infrared surveillance, imaging, remote sensing, and hyperspectral imaging; effects of solar activity, magnetic storms and nuclear explosions on the Earth's atmosphere, ionosphere and magnetosphere; effects of electromagnetic and particulate radiations on space systems; space instrumentation, design fabrication and test; environmental chemistry, trace detection; atmospheric chemical reactions, atmospheric optics, light scattering, state-specific chemical reactions and radiative signatures of missile plumes.

Center for Microtechnology: Microelectromechanical systems (MEMS) for space applications; assessment of microtechnology space applications; laser micromachining; laser-surface physical and chemical interactions; micropropulsion; micro- and nanosatellite mission analysis; intelligent microinstruments for monitoring space and launch system environments.

Office of Spectral Applications: Multispectral and hyperspectral sensor development; data analysis and algorithm development; applications of multispectral and hyperspectral imagery to defense, civil space, commercial, and environmental missions.